https://doi.org/10.1016/j.canlet.2024.216870

Circulating tumor cells with metastasis-initiating competence survive fluid shear stress during hematogenous dissemination through CXCR4-PI3K/AKT signaling

Ying Xin[1,2,3], Bing Hu[1,2,3], Keming Li[1,2], Guanshuo Hu[1,2,3], Cunyu Zhang[1,2,3], Xi Chen[1,2], Kai Tang[1,2], Pengyu Du[1,2], Youhua Tan[1,2,3]*

[1] The Hong Kong Polytechnic University Shenzhen Research Institute, Shenzhen (518000), China

[2] Research Institute of Smart Ageing, The Hong Kong Polytechnic University, Hong Kong (999077), China

[3] Department of Biomedical Engineering, The Hong Kong Polytechnic University, Hong Kong (999077), China

* Correspondence: youhua.tan@polyu.edu.hk

Keywords: fluid shear stress, mechanotransduction, metastasis-initiating cells, hematogenous dissemination

Abstract

To seed lethal secondary lesions, circulating tumor cells (CTCs) must survive all rate-limiting factors during hematogenous dissemination, including fluid shear stress (FSS) that poses a grand challenge to their survival. We thus hypothesized that CTCs with the ability to survive FSS in vasculature might hold metastasis-initiating competence. This study reported that FSS of physiologic magnitude selected a small subpopulation of suspended tumor cells *in vitro* with the traits of metastasis-initiating cells, including stemness, migration/invasion potential, cellular plasticity, and biophysical properties. These shear-selected cells generated local and metastatic tumors at the primary and distal sites efficiently, implicating their metastasis competence. Mechanistically, FSS activated the mechanosensitive protein CXCR4 and the downstream PI3K/AKT signaling, which were essential in shear-mediated selection of metastasis-competent CTCs. In summary, these findings conclude that CTCs with metastasis-initiating competence survive FSS during hematogenous dissemination through CXCR4-PI3K/AKT signaling, which may provide new therapeutic targets for the early prevention of tumor metastasis.

Introduction

Tumor cells disseminate from the primary lesion to distal organs mainly through the hematogenous route [1]. Although millions of tumor cells are shed from a primary tumor of 1 cm size and infiltrate into vasculature every day, the majority of circulating tumor cells (CTCs) cannot survive hematogenous dissemination under various rate-limiting factors, such as oxidative stress, anoikis, immune surveillance, and fluid shear stress (FSS) [2, 3]. Consequently, less than 0.02% of CTCs may eventually generate secondary tumors [4-6], suggesting the inefficiency of the metastatic process. Nevertheless, metastasis is still a common and major threat to the patients with cancer: approximately 20-30% of breast cancers diagnosed at early stages are expected to progress to metastatic disease [7] that accounts for more than 90% of cancer deaths [8]. These findings implicate the existence of a tiny subpopulation of CTCs with the ability to survive the entire dissemination cascade and establish metastatic colonization at distal organs, which have been proposed as metastasis-initiating cells (MICs) [9].

MICs are believed to be a rare subpopulation of tumor cells with unique traits that enable them to complete the entire metastatic process, including proliferative ability, resistance to apoptosis and therapy, metabolic adaptation, self-renewal, exit from dormancy, escape from immune surveillance, and cellular plasticity [9]. Therefore, it is crucial to isolate these scarce cells for comprehensive characterization in order to develop novel therapeutic strategies. Currently, two mainstream methods have been adopted for this purpose. The first approach is based on the expressions of cell surface markers, including CD36 for oral carcinoma [10], L1CAM for colorectal cancer [11], tenascin C [12], CD24/CD90 [13], CD44/CD47/MET [14], ALDH1A3 [15], and CXCR3 [16] for breast cancer. Since surface proteins dynamically evolve during tumor progression, this method is highly dependent on cancer stage and cancer type/subtype, which challenges their wide applications for MIC enrichment across different cancer types. The other is an *in vivo* method that transplants tumor cells into animals for metastases formation and isolates the cells from metastatic tumors after several rounds of passage [17]. This method is time-consuming, and the isolated cells usually metastasize to specific organs with poor enrichment of MICs. Therefore, a novel and generic strategy that enables reliable isolation of MICs is highly desirable.

As MICs have been proposed as the bona fide "seeds" that initiate metastatic tumors, they must hold the ability to survive hematogenous dissemination, including FSS in vasculature. Recent studies show that tumor cells in suspension can sense and respond to FSS [18-21]. For example, the viability and proliferation of suspended colon tumor cells depend on the magnitudes of FSS and circulation time [22]; FSS decreases the viability of suspended prostate cancer cells possibly via cell membrane damage and reduced membrane repair [23]; high FSS induces significant apoptosis but facilitates the migration and extravasation of the surviving CTCs [24, 25]; increasing FSS disaggregates CTC clusters and reduces their viability [26]. Nevertheless, multiple types of tumor cells exhibit resistance to shear-induced destruction: suspended breast cancer cells resist shear-induced apoptosis and necrosis, which depends on Lamin A/C [27]; prostate tumor cells evade shear-induced plasma membrane damage in a RhoA-dependent manner [28]; breast and lung cancer cells that resist FSS upregulate desmocollin-2 and plakophilin-1, which promote the formation of CTC clusters in circulation and facilitate tumor metastasis [3]; laminar FSS upregulates atonal bHLH transcription factor 8 in colorectal cancer cells, which promotes the survival and metastasis of CTCs via HK2-mediated glycolysis [29]; CTCs within the microvasculature upregulate pannexin-1 channel, which enhances their survival via ATP release [30]. Therefore, CTCs can sense and resist FSS in hematogenous dissemination. However, whether and how FSS in vasculature influences the metastasis-initiating ability of CTCs remain unclear.

This study hypothesized that FSS during hematogenous dissemination could select a subpopulation of CTCs with metastasis-initiating ability. Toward this goal, an *in vitro* circulatory system was developed to mimic FSS in the vascular system. After the optimization of the selection conditions, tumor cells with metastasis-initiating competence were harvested and their properties were characterized, including cancer stemness, metastatic potential, cell plasticity, and biophysical properties. Further, the mechanotransduction signaling by which FSS enriched MICs were elucidated.

Results

FSS enriches a subpopulation of CTCs with enhanced stemness, migration, and invasion

CTCs experience varying levels of FSS during hematogenous dissemination. In human vasculature, the mean FSS is 1-4 dyne/cm^2 in vein, 10-20 dyne/cm^2 in capillary, and 4-30 dyne/cm^2 in artery [31]. The half lifetime of CTCs in patients is estimated to be 1-3 h, and almost all CTCs undergo either apoptosis or extravasation within 12 h after entering the vasculature [32]. To mimic such shearing condition, a microfluidic system we developed previously was adopted to circulate breast cancer cells in suspension under different levels of FSS for various durations (Fig. 1a). Our previous studies have illustrated that the viability of suspended tumor cells gradually decreases along with the increase of FSS and circulation time [18, 33, 34]. To determine the experimental conditions for the enrichment of tumor cells with metastasis-initiating competence, multiple magnitudes of FSS (5, 10, 20, and 30 dyne/cm^2) and durations (0, 4, 8, and 12 h) were adopted to circulate tumor cells in suspension (Fig. 1a). The stemness and motility of the surviving cells, typical features of MICs, were compared to optimize the selection parameters. Among 0, 5, and 10 dyne/cm^2 FSS, tumor cells after the treatment of 10 dyne/cm^2 FSS for 12 h displayed the highest migration and colony formation ability and up-regulated the genes related to stemness and metastasis (Fig. S1a-c). Similarly, among 0, 20, and 30 dyne/cm^2 FSS, suspended cells surviving 20 dyne/cm^2 shear treatment for 12 h exhibited the highest malignancy (Fig. S1d-f). We further compared these two optimized conditions and found that breast cancer cells after the 12-h circulation under 20 dyne/cm^2 FSS acquired the highest migration (Fig. S2a), invasion (Fig. S2b), self-renewing ability (Fig.S2c), and stemness-related markers (Fig. S2d and e). Thus, the optimal selection condition was determined as 20 dyne/cm^2 shear treatment for 12 h. Note that compared to cancer cells, almost all the healthy breast epithelial cells MCF-10A underwent apoptosis under 20 dyne/cm^2 shear stress (Fig. S2f and g), suggesting that healthy cells are more sensitive to shear-induced death.

Further, the metastasis-initiating ability of tumor cells surviving under the optimal selection condition (shear-selected MICs or ssMICs) was characterized. After the survival in vasculature, CTCs need to re-

attach to the endothelium before extravasation. ssMICs were prone to adhere to the endothelial monolayer much faster than that of tumor cells selected by 0 dyne/cm^2 FSS (suspension control) and control tumor cells (Fig. 1b). After 8 h, there were more stably adhered ssMICs compared to the other two groups. Subsequent to re-adhesion, it is necessary for CTCs to extravasate through the endothelium into distal organs. ssMICs displayed ~75% and 50% increase in the trans-endothelial migration ability compared to suspension control and control cells (Fig. 1c), respectively. After extravasation, disseminated tumor cells need to migrate through the basement membrane and parenchyma before the seeding in the metastasized organ. ssMICs increased their migration ability through the confinement by 89% and 200% (Fig. 1d), and displayed more than 60% and 47% higher invasion index in 3D collagen than suspension control and control cells (Fig. 1e), respectively. These findings were supported by the upregulation of the metastasis-related gene CXCR4 (Fig. 1i). Upon the arrival at the target organs, self-renewal or stemness is important for these tumor cells to thrive and generate metastatic tumors. ssMICs formed 64-90% more tumor colonies in 3D soft agar than the other two groups (Fig. 1f). Further, shear treatment considerably increased the percentages of CD133+ and CD44+/CD24- subpopulations (Fig. 1g and h), which are usually utilized to mark breast cancer stem cells [35, 36], and upregulated stemness markers (e.g., CD133, CD44, and Bmi-1) (Fig. 1i and j). Note that 3D microenvironments, such as trans-endothelial model and 3D collagen/agar gels for the test of invasion/self-renewal, are presumably better than 2D substrates in mimicking the *in vivo* milieu. These results suggest that ssMICs acquire high stemness. In addition, the enhancement of metastasis-initiating ability after shear treatment was also observed in several other breast cancer cells (e.g., MDA-MB-231, MCF-7, and 4T1) and three other types of cancer, such as liver cancer (HepG2), osteosarcoma (MG63), and lung cancer (A549; Fig. S3d-g), suggesting that the impact of FSS on metastatic competence may be generalized across multiple cancer types. In summary, all these findings demonstrate that shear-selected tumor cells exhibit metastasis-initiating ability *in vitro*.

Shear-selected tumor cells exhibit metastasis-initiating ability *in vivo*

The metastatic competence of ssMICs was further examined *in vivo*. To test the ability to generate local lesions, tumor cells were inoculated subcutaneously into nude mice, where tumor-initiating cells (TICs), breast cancer cells after mammosphere culture, were utilized as a positive control. Compared to control cells, ssMICs and TICs generated the largest local tumors after implantation (Fig. 2a), followed by suspension control. The weights of tumor xenografts generated by TICs and ssMICs were much higher than the control group (Fig. 2b). To better mimic the microenvironment at the primary site, all tumor cells were implanted into the mammary fat pad of female nude mice. The average size of the tumors generated by ssMICs was significantly larger than the control group (Fig. 2c and d). When the tumor volume reached ~500 mm^3, the primary tumors were surgically resected to facilitate metastasis. Higher metastatic burden was observed in the ssMICs group compared with suspension control and control tumor cells (Fig. 2e and f). The luminescence signal of ssMIC-generated metastases was more than 3-fold higher than those developed by the other two groups (Fig. 2g). Besides, the metastasis incidences of ssMICs in brain and bone were higher than that of suspension control and control tumor cells (Fig. 2h). Further, the metastatic potential was examined in the intracardiac xenograft model. ssMICs exhibited higher metastatic potential than control cells and suspension control (Fig. S4a, b, and d). The metastasis incidences of ssMICs in the brain and bone were noticeably elevated (Fig. S4c). In summary, all these findings demonstrate that ssMICs acquire enhanced tumor formation ability and metastatic potential *in vivo*, reflecting their metastasis-initiating competence.

ssMICs display characteristic biophysical properties and cellular plasticity

Tumor cells with different metastatic potential exhibit distinct biophysical properties [37] [38], suggesting the correlation between malignancy and cellular biophysics. Our recent work has demonstrated that the mechanical alterations of tumor cells during progression drive tumorigenic and metastatic potential. We thus further characterized the biophysical properties of ssMICs. Since the majority of breast cancer metastases occur in bone (~67%), lung, and liver (~30%) [41], polyacrylamide (PA) gels with the stiffnesses of 5 and 35 kPa were adopted to mimic the mechanics of these tissues [42]. ssMICs showed much higher proliferation on such two substrates compared to suspension control

and control cells (Fig. 3a), suggesting the mechanoadaptation of these cells to the mechanical microenvironments of the metastasized organs. Living cells actively explore and/or remodel the surrounding microenvironment by generating and exerting contractile forces. Compared to the other two groups, ssMICs generated 134-165% higher traction force on 35 kPa PA gels (Fig. 3b), which might partially explain the enhanced cell proliferation. Further, the stiffness measurement by atomic force microscopy (AFM) illustrated that ssMICs were much softer than suspension control cells and control tumor cells (Fig. 3e), which was further supported by the reduction of F-actin in ssMICs (Fig. 3c and d). These findings suggest that ssMICs generate elevated contractile forces and exhibit enhanced cell proliferation but reduced cytoskeleton and mechanical stiffness.

Cellular plasticity is one unique feature of MICs, and has been proposed to endow tumor cells phenotypical change between the differentiated state and the stem-like state for long-term growth [43] and adapt to various microenvironments during the metastatic process [44]. The percentage of the stem-like CD133+ subpopulation in ssMICs was three times higher than suspension control and ten times higher than control cells (Fig. 3f). After plating these cells on petri dishes for 7 days, this percentage decreased dramatically to the level that was comparable to that of control groups. Similarly, the stemness-related markers (CD44, Sox2, and CD133) and metastasis-related marker CXCR4 were up-regulated in ssMICs and then down-regulated after the culture on petri dishes for 7 days (Fig. 3g). Further, F-actin, phosphorylated myosin light chain (p-MLC), and cellular stiffness of ssMICs were lower and tended to increase to the similar or even higher level as control cells after 3- and 6-day culture on glass (Fig. 3h-j). These results demonstrate that ssMICs exhibit high cellular plasticity in stemness and biophysical properties.

FSS enriches ssMICs through CXCR4

We have demonstrated that CTCs surviving FSS during hematogenous dissemination exhibit metastasis-initiating ability both *in vitro* and *in vivo*. We then asked how blood FSS selected these malignant ssMICs. Tumor cells are able to perceive external mechanical stimuli and further convert

them into biochemical signals through mechanotransduction [45]. Since CTCs were in suspension state under FSS, we assumed that the integrin-mediated adhesion signaling might not be critical in mechanosensing in this context. The promising candidates might include those cell membrane proteins that are both mechanosensitive [46, 47] and essential in tumor metastasis, including CXCR4 [48, 49]. Our earlier results showed that the metastasis-related gene *CXCR4* was upregulated in ssMICs (Fig. 1i and Fig. 3g). We further explored the influence of FSS on CXCR4 at the protein level. Both immunofluorescence (Fig. 4a; Fig. S5a and b) and immunoblotting (Fig. 4b; Fig. S5c) results illustrated that the CXCR4 protein level was notably higher in ssMICs compared with suspension control and control tumor cells. The percentage of CXCR4+ subpopulation was elevated from 49.2% in control tumor cells, 57.9% in suspension control, to 71.5% in ssMICs (Fig. 4c). To examine the role in shear-mediated ssMIC selection, CXCR4 was inhibited by siRNA (Fig. S5d) or the inhibitor AMD3100 (Fig. S5g) before circulation in FSS, which had no obvious cytotoxicity on tumor cells (Fig. S5e and h). Inhibiting CXCR4 signaling reduced the survival of suspended tumor cells under FSS (Fig. S5f) and decreased the migration and self-renewing ability of tumor cells after the treatment of both 0 and 20 dyne/cm^2 FSS (Fig. 4d-i). In particular, silencing CXCR4 under FSS suppressed cell migration and colony formation to the levels of suspension control (Fig. 4e and f; Fig. 4h and i). These results suggest that FSS selects these malignant ssMICs through the mechanosensitive CXCR4 signaling. Note that when CXCR4 was silenced, FSS still enhanced the migration and self-renewal of suspended tumor cells (Fig. 4e and f; Fig. 4h and i), suggesting that except CXCR4, other mechanosensitive proteins may also mediate the effect of shear force on tumor cells. Further, inhibiting CXCR4 in ssMICs (Fig. S5i-l) significantly reduced their migration and colony formation ability (Fig. 4j-l). Pharmacological suppression of CXCR4 noticeably reduced the invasion ability of these cells (Fig. 4m). All these results suggest that CXCR4 not only mediates the shear-induced MIC selection but also plays critical roles in the metastasis-initiating ability of the shear-selected tumor cells.

FSS selects ssMICs via CXCR4-PI3K-AKT signaling

We next dissected how FSS selected ssMICs via CXCR4. Shear treatment notably increased the percentage of CXCR4+ subpopulation (Fig. 4c), which might be explained by the possible reason that CXCR4- cells were more susceptible to shear-induced destruction and/or converted into CXCR4+ phenotype. To test these two possibilities, breast cancer cells were sorted into CXCR4- and CXCR4+ subpopulations, which were then exposed to FSS. Indeed, CXCR4+ cells were more resistant to shear-induced apoptosis (Fig. 5b), which was consistent with the earlier finding (Fig. S5f). For CXCR4- tumor cells, the percentage of CXCR4+ subpopulation was increased from 2.8% to 34.5% under 0 dyne/cm^2 FSS, and to 61.2% under 20 dyne/cm^2 FSS (Fig. 5a). For CXCR4+ cells, the percentage of CXCR4+ subpopulation was maintained after shear treatment. Further, CXCR4+ tumor cells were more migrative and self-renewing than CXCR4- cells and the migration and self-renewal abilities of both subpopulations were significantly enhanced after shear treatment (Fig. 5c and d). Shear-treated CXCR4+ cells showed comparable self-renewal and higher migration compared to the shear-treated CXCR4- cells. These results indicate that FSS selects MICs through both enriching CXCR4+ cells with survival and metastatic advantage and facilitating the phenotypic conversion of CXCR4- cells into CXCR4+ cells.

CXCR4 is a mechanosensitive membrane protein with two classic downstream signaling [46, 47, 50]: PI3K-AKT and MAPK-ERK pathways [51, 52]. ssMICs up-regulated the expressions of PI3K and AKT but not ERK1 and ERK2 compared with suspension control and control tumor cells (Fig. S6a and b). Inhibition of CXCR4 signaling through genetic and pharmacologic treatment restored the elevated expressions of PI3K and AKT to the control level but had minimal effect on ERK under shear treatment (Fig. S6c-f). These results suggest that CXCR4 may sense shear force through PI3K-AKT pathway in suspended tumor cells. Further, the shear-induced activation of PI3K-AKT signaling was examined at the protein level. FSS had no obvious influence on the total PI3K protein but facilitated its phosphorylation and activation in both SKBR3 and 4T1 cells (Fig. 5e; Fig. S6g, h, and l). Note that SKBR3 cells are HER2+ and exhibit aberrant activation PI3K/AKT signaling [53], while 4T1 cells are triple negative and have low level of PI3K/AKT activation [54]. The promotive effect of FSS on PI3K activation in both SKBR3 (high level of PI3K activation) and 4T1 (low level of PI3K activation)

possibly excluded the potential influence of other causes on excess PI3K activation. To explore the roles of PI3K-AKT signaling, pharmacologic treatment was adopted to modulate the activity in both SKBR3 and 4T1 cells (Fig. S6i and j). Inhibiting PI3K pathway decreased the migration and self-renewal ability of breast cancer cells under 20 dyne/cm^2 FSS by ~60% and 13%, and slightly reduced these properties under suspension treatment (Fig. 5f-h; Fig. S6m). Note that even when the PI3K signaling was suppressed, the migration and stemness of tumor cells were still higher under 20 dyne/cm^2 FSS than 0 dyne/cm^2 suspension, suggesting that FSS might regulate tumor cell motility and self-renewal through not only PI3K-AKT pathway but also other unknown mechanisms. When CXCR4 was silenced, activation of PI3K signaling by insulin receptor substrate (Tyr608) peptide rescued cell survival (Fig. S6k), migration (Fig. 5i and j), and colony formation ability (Fig. 5i and k) under shear treatment. In addition, higher level of CXCR4 in primary breast tumors was associated with worse metastasis-free survival (Fig. S6n), suggesting the clinical significance of CXCR4 signaling in tumor metastasis. Taken together, these results demonstrate that FSS enriches MICs through the CXCR4-PI3K-AKT signaling.

Discussion

Metastasis remains the major cause of cancer-related death, though significant advances in targeted therapies have been made in recent years [55]. Previous studies have emphasized the significance of various critical factors in metastasis [56], such as genomic mutations, local niches within primary tumors, and different microenvironments encountered during metastasis. Despite these well-known biochemical factors, the roles of mechanical cues in malignancy have been increasingly appreciated [57, 58]. As a major route of metastasis, tumor cells spread to secondary sites mainly through hematogenous dissemination [8], where CTCs experience varying levels of FSS. Our recent studies together with many others have shown that FSS of physiologic magnitudes eliminates the majority of CTCs in vasculature [18, 20, 22, 34, 59], while a small subpopulation can persist and survive during this process [3, 23, 24, 27, 28]. Since metastasis is a multi-step and sequential process, tumor cells, in particular MICs (the initiators of secondary lesions) must survive the entire metastatic cascade [9], including vascular FSS,

before they reach targeted organs to generate clinically detectable metastases. However, how FSS during hematogenous dissemination influences the metastatic-initiating competence of CTCs remains unclear.

Our previous research shows that the survival of suspended tumor cells within circulation depends on the levels of FSS and circulation time [59], suggesting that tumor cells in suspension can sense and respond to shear force. Based on this mechano-perception, the current study reports that breast cancer cells that survive the optimized shear selection condition (e.g., 20 dyne/cm^2 FSS for 12 h) exhibit metastasis-initiating competence, including enhanced adhesion to the endothelium, trans-endothelial migration, migration, invasion, stemness, cellular plasticity, and unique biophysical properties. Importantly, these shear-selected MICs or ssMICs have the ability to efficiently generate local tumors in both subcutaneous and orthotopic xenograft models and initiate distal metastases both after the surgical removal of the primary tumors and after intracardiac injection. These findings suggest that shear treatment, a single rate-limiting factor during hematogenous metastasis, is able to select a subpopulation of CTCs with metastasis-initiating ability, which is applicable to multiple types of cancer, such as breast, liver, bone, and lung cancer. In line with our results, previous studies show that shear treatment reprograms the metabolism of CTCs and promotes their metastatic potential in prostate and breast cancer [60]. FSS induces epithelial-to-mesenchymal transition and upregulates the stemness markers, which further enhance the malignancy of lung cancer cells [61]. High RhoA and actomyosin activity protects CTCs from shear-induced destruction [28] and may elevate the contractility of the surviving ssMICs. Desmocollin-2 and plakophilin-1 confer the survival advantage of tumor cells in blood shear flow and promote cluster formation and metastasis via fibronectin/integrin β1/FAK/Src/MEK/ERK/ZEB1 signaling [3]. Our earlier findings show that FSS promotes epithelial-to-mesenchymal transition of suspended tumor cells via Jun N-terminal kinase (JNK) signaling, which promotes their survival in blood flow [34]. We expect that the combination of FSS with other rate-limiting factors during metastasis, such as immune surveillance (e.g., natural killer cells) and the barrier of extravasation, may further increase the enrichment of MICs [62].

Cells are able to sense and respond to mechanical stimulations through mechanotransduction, which has been intensively investigated for the cells that are adhered to solid substrates (adherent cells) [63]. However, how the cells in suspension (lack of anchorage) perceive mechanical cues, such as FSS, remains incompletely understood. Our study reports that shear treatment upregulates the expression of CXCR4, one of the G protein-coupled receptors (GPCRs) family [64, 65], which enhances the resistance of suspended tumor cells to shear-induced destruction. FSS promotes the mobility and stemness of suspended tumor cells, which can be rescued to the control levels by the inhibition of CXCR4, suggesting that CXCR4 may function as a mechanosensitive protein in mediating the effect of shear force on suspended cells. Note that when CXCR4 is silenced, shear force can still mildly promote the migration and stemness of tumor cells, implicating that some other proteins, such as other GPCRs (e.g., GPR68) and ion channels (e.g., Piezos) [66], may function as mechanosensors in the shear-mediated selection of ssMICs. For example, GPR68 is crucial in shear stress-induced calcium influx of breast cancer cells [67]. ATOH8 is responsive to FSS, facilitating colorectal cancer cell metastasis [29]. Red blood cells sense FSS via Piezo1, which further leads to the generation of extracellular vesicles [68]. Further, FSS enriches ssMICs by preferentially eliminating CXCR4- cells and facilitating the phenotypic conversion of CXCR4- cells into CXCR4+ cells, and enhances the malignancy of both subpopulations via the downstream PI3K-AKT pathway. The migration, invasion, and stemness of ssMICs highly depend on CXCR4 expression. In line with these findings, previous studies report the roles of CXCR4 in the mechanotransduction of adherent cells: breast cancer cells exhibit much higher unbinding forces of CXCR4 than normal mammary cells on 350-kPa hydrogels [47]; matrix stiffness promotes the proliferation, epithelial-to-mesenchymal transition, and stemness of liver cancer cells through CXCR4-mediated ubiquitin domain-containing protein 1 and YAP signaling [46]; interstitial flow increases the invasion of glioblastoma [50] and liver cancer cells via CXCR4 [69]. In addition, previous findings show the promotive effect of CXCR4 on metastasis [48, 49] and a positive association between CXCR4 expression and poor patient survival [70, 71]. Nevertheless, further efforts are still required to elucidate the detailed mechanotransduction process in suspended cells. In particular, it

remains unclear whether adherent and suspended cells respond to the same mechanical cues similarly or distinctly.

This study has achieved the shear-mediated selection of MICs with several limitations, which need to be addressed in future. First, the *in vitro* circulatory system that is adopted in the current study can only partially recapitulate the complexity of the real vascular microenvironment due to lack of the interactions with blood and immune cells and no consideration of different sizes of capillaries (~4 μm), venules (10-30 μm), and arteries (0.2-20 mm) [72]. It is known that blood cells, such as platelets, can interact with CTCs and thus protect them from shear-induced apoptosis [73]. Immune cells, such as natural killer cells, effectively eliminate CTCs in the short lifetime within the vasculature [74]. In addition, the plasma viscosity of breast cancer patients is 1.32 mPa.s, which is higher than that of the healthy group [75] and can influence the shearing condition in circulation. Second, suspended tumor cells may represent certain but not all the essential features of bona fide CTCs. However, CTCs are very scarce in the peripheral blood of cancer patients (1-10 CTCs per ml blood) [76], which challenges the usage of many patient-derived CTCs in the study, although the latest developed CTC lines may alleviate this concern to some extent [77].

Conclusion

In summary, this study demonstrated that FSS during hematogenous dissemination selected a small subpopulation of CTCs with metastasis-initiating ability. The selected cells held the essential traits for the efficient generation of local tumors and distal macroscopic metastases and possessed unique biophysical properties. The shear-mediated selection of ssMICs was achieved via the mechanosensitive protein CXCR4 and the downstream PI3K/AKT signaling. In particular, FSS preferentially eliminated CXCR4- cells, facilitated the phenotypic conversion of CXCR4- cells into CXCR4+ cells, and promoted the malignancy of both CXCR4- and CXCR4+ cells. Silencing CXCR4 notably reduced the mobility and stemness of ssMICs. Taken together, this study provides the evidence to conclude that FSS, as a single rate-limiting factor in vasculature, can select the rare and malignant MICs from CTCs

through CXCR4-PI3K/AKT signaling. This may provide a novel strategy for MIC enrichment and characterization and offer new therapeutic targets for the mechanotargeting of CTCs in vasculature.

Materials and methods

Cell culture: Breast cancer cell lines (MDA-MB-231, MCF-7, SKBR3, and 4T1), liver cancer cell line HepG2, human osteosarcoma cell line MG-63, human kidney epithelial cell line 293T, and human endothelial cell line HUVEC were obtained from American Type Culture Collection (ATCC). MDA-MB-231 cells, SKBR3 cells, HepG2 cells, MG63 cells, and 293T cells were cultured in the complete culture medium that was composed of Dulbecco's Modified Eagle Medium (DMEM; HyClone, Logan, UT), 10% fetal bovine serum (FBS) (HyClone), and 1% penicillin/streptomycin (HyClone). MCF-7 and 4T1 cells were cultured in RPMI-1640 medium (Gibco) supplemented with 10% FBS and 1% penicillin/streptomycin. HUVEC cells were cultured in Endothelial Cell Medium (ECM) (ScienCell Research Laboratories). Cells were cultured in a culture dish at 37°C and a 5% CO_2 incubator and passaged every three days using 0.25% Trypsin (HyClone).

Circulatory system: The circulatory system was composed of a peristaltic pump (P-230, Harvard Apparatus), silicone micro-tubing (1.5 m in length, PharMed), and a 10 ml syringe. The system could produce FSS at the physiological levels of human circulation system (0-30 dyne/cm^2). According to Poiseuille's law, wall shear stress τ (dyne/cm^2) in the tubing was calculated by $\tau=4\mu Q/(\pi R^3)$, where Q was the flow rate (from 0.37 to 3.2 ml/min), μ was the dynamic viscosity of the fluid (0.01 dyne*s/cm^2 for cell culture medium), and R was the radius of the tube (0.255 mm). Before the experiments, the whole system was sterilized with 3 ml of 75% ethanol and then washed with 3 ml phosphate buffered saline (PBS, HyClone). 3ml of 1% bovine serum albumin (BSA, VWR Life Science) solution was then added to the circulatory system to reduce the possible cell adhesion to a silicone tube or syringe. The different magnitudes of shear stress were achieved by altering the flow rate of the pump. During shear stress treatment, 2 ml of single cell solution ($2*10^5$ cells/ml or $2*10^6$ cells/ml) was injected into the

circulatory system and exposed to 0, 5, 10, 20, and 30 dyne/cm^2 shear stress for 0-12 h in the cell culture incubator at 37°C and 5% CO_2.

Polyacrylamide (PA) gel preparation and cell morphology quantification: Polyacrylamide gels were prepared based on the previous protocol [33]. 35 kPa PA gels were made by mixing 0.3% bis-acrylamide crosslinker and 10% acrylamide (Bio-Rad). The gels were activated under UV light with Sulfo-SANPAH (Pierce) and then immersed with 200 μg/ml collagen solution at 4°c for 18 h. The polyacrylamide gels were sterilized before use. Control tumor cells and tumor cells under different stimulations were plated on 35 kPa gels for 12 h and unattached cells were gently removed before analysis. At least 50 cells/conditions were imaged under an inverted microscope (Nikon). Cell spreading area and aspect ratio were analyzed using ImageJ (NIH).

Flow cytometry and fluorescence-activated cell sorting (FACS): After various treatments, tumor cells were collected and washed with PBS. Several antibodies, such as CD24 (Abcam), CD44 (Abcam), CD133 (Biolegend), and CXCR4 (Abcam), were utilized for cell labelling. Antibodies were diluted in PBS containing 2% FBS as recommended by the manufacturer. Tumor cells were stained with diluted antibody solution in the dark for at least 30 min on ice and then washed with PBS for 3 times. At last, cells were resuspended in PBS containing 2% FBS. The cell solution without antibody staining was utilized as a negative control. The percentage of marker expression was analyzed by BD FACSVia™ flow cytometer (BD Biosciences) and at least 10000 cells were analyzed under each condition. For FACS, tumor cells were labelled with specific antibodies. The FACS machine (BD FACSAria III Cell Sorter, BD Biosciences) was calibrated and set up with the appropriate laser and filter settings to detect and separate the fluorescently labelled cells. The cell solution was then introduced into the FACS machine. As the cells passed through the laser beam, the positive and negative subpopulations of cells were sorted based on their fluorescence intensity.

Transwell migration and invasion assay: For transwell migration assay, $1*10^5$ of tumor cells were collected, re-suspended in 200 μl DMEM plus 1% FBS medium (or RPMI-1640 plus 1% FBS medium), and added on the upper layer of a Transwell insert, while 500 μl of the complete medium was added to the bottom chamber. The cells could migrate from the upper side to the lower side of the Transwell

chamber (Corning) at 37°C. After 24 h, the cells on the upper side were gently removed with a cotton swab. Crystal violet powder (Solarbio) was dissolved in 20% EtOH and the remaining cells on the other side of the chamber were stained with 0.5% crystal violet solution. After washing away the excess staining solution, the number of migrated cells was counted under a 10x inverted microscope (Nikon). In Transwell invasion assay, the upper side of a Transwell insert with 8 μm pores was pre-treated with 100 μl of 1mg/ml Matrigel (Corning) and incubated at 37°C for 1 h. Then, 100 μl of cell suspension containing $1*10^5$ cells was added on top of the concreting Matrigel. Next, 500 μl of the complete medium was added to the lower chamber. The cells invaded the Matrigel and reached the lower side of the chamber at 37°C. After 24 h, a cotton swab was utilized to remove the cells as well as the Matrigel on the upper side of the Transwell. The remaining cells on the other side of the chamber were stained with 0.5% crystal violet solutions. After washing away the excess staining solution, the number of invaded cells was counted and imaged under a 10x inverted microscope.

Trans-endothelial migration assay: $5*10^4$ of HUVEC cells were plated on the upper layer of a Transwell insert (Corning) with 8 μm pores and cultured in ECM medium for 2-3 days to form a confluent monolayer. Then, $1*10^5$ of fluorescent-labelled tumor cells re-suspended in 200 μl DMEM plus 1% FBS medium were added to the top of HUVEC cells. After 48 h, tumor cells on the top chamber were removed by a cotton swab and those tumor cells which migrated through the endothelium were imaged and counted under a 10x inverted microscope.

Soft agar colony formation assay: The soft agar colony formation assay is an *in vitro* method to evaluate cell stemness and carcinogenesis based on anchorage-independent cell growth [78]. 2ml of 1% low gelling temperature agarose (Sigma Aldrich) solution was added into each well of 6-well plates and kept at room temperature for 15 min to get a concrete layer of soft agar on the bottom. Then, 3.7 ml of 3% agarose, 6.3 ml of the complete culture medium, and 1 ml FBS were mixed to prepare 0.8% agarose mixture. 1×10^4 cells/ml cell solution was mixed 1:1 with 0.8% agarose mixture. 2 ml of this cell and agarose mixture was added to the top of the bottom layer of each well. The 6-well plate was kept at 4°C for 10 min for the gel solidification and then incubated at a 37°C incubator. 300 μl of the complete medium was added every 4 days. After incubating for 14-21 days, the colonies were stained with 0.005%

Crystal Violet and washed with distilled water. The number of colonies with the diameter larger than 50 μm was counted and imaged by ChemiDoc™ MP Imaging System (BIO-RAD).

Cell adhesion assay: 50,000 HUVEC cells were added to the gelatin-coated 24-well plate and cultured in an incubator for 2-3 days until they reached a confluent monolayer. Tumor cells were labelled with CellTracker Red CMTPX (Thermo), and $1*10^5$ these labelled cells were re-suspended in 1ml ECM medium (ScienCell Research Laboratories). The culture medium of HUVEC cells was carefully removed and 1 ml of tumor cell solution was slowly added on top of the HUVEC monolayer. For each condition, 2-3 wells were prepared, and the culture medium was carefully removed after being co-cultured for 30 min, 1 h, 2 h, 4 h, and 8 h, respectively. Cells were gently washed with PBS for 2-3 times and the adhered tumor cells were counted under a fluorescent microscope.

Three-dimensional (3D) collagen invasion assay: $1*10^4$ of control 4T1 cells and 4T1 cells after shear treatment were suspended in 20 μl culture medium and placed on the lid of the culture dish for 2 days to form an intact tumor spheroid. 1 mg/ml collagen mixture was prepared with collagen solution (Corning), 10× RPMI (Gibco), PBS (Hyclone), and insulin (Sigma Aldrich). NaOH was added into the collagen solution to adjust the pH of the mixture ranging from 7.4-7.6. 50 μl of collagen mixture was added to one well of a 96-well plate and incubated at 37° for 30 min to form the bottom layer of collagen. Then, the tumor spheroids were collected and resuspended in 80 μl of collagen mixture, which was added onto the top of the bottom collagen layer and incubated at 37° for 30 min. 50 μl of culture medium was added on top of the collagen gel. Tumor spheroids were imaged at 0, 12, and 24 h, respectively. The invasion area was analyzed by ImageJ and the invasion index was calculated as invasion index= (invasion area at 12 h or 24 h)/initial spheroid area.

Cell stiffness measurement: The Bruker Catalyst atomic force microscope (AFM) (Bruker, Billerica, MA) combined with an inverted microscope (Nikon, Tokyo, Japan) was utilized to measure tumor cell stiffness. The AFM probe consisted of silicon nitride cantilevers and tips with 0.02 N/m spring constant. Before the experiment, the sensitivity and spring constant of the probe were calibrated in culture medium. Tumor cells surviving 0 or 20 dyne/cm^2 shear stress were collected and plated on a petri-dish and incubated at 37°C for 12 h. Tumor cells were washed gently to remove unattached cells before the

experiment. Breast cancer cells were visualized under the microscope and indented by the AFM tip. The indentation depth was 500 nm, and the tip velocity was 1 mm/s at room temperature. For each condition, at least 50 cells were measured, and the cell Young's modulus was calculated by fitting the force-indentation curves with the Sneddon model.

Cell traction force measurement: Cellular traction force was measured using the traction force microscopy technique [79]. Tumor cells surviving 0 or 20 dyne/cm^2 shear stress and control tumor cells were seeded at low density on 35-kPa PA gels, the apical surface of which was embedded with 200 μm fluorescence beads (Invitrogen). The outline of cancer cells was captured by an inverted microscope in the bright field. Images of fluorescence beads under the cells were taken before and after detaching the cells from the gels and utilized to compute the displacement field of the beads, from which cellular traction force was calculated based on the inverse Boussinesq mathematical model.

Quantitative RT-PCR: Tumor cells after different treatments were collected and washed with PBS to remove excess culture medium. The total mRNAs were extracted by E.Z.N.A.® Total RNA Kit I (Omega) and the concentration of mRNA was determined by NanoDrop™ (Thermo). Complementary DNA was synthesized using RevertAid First Strand cDNA Synthesis Kit (Thermo) following the manufacturer's manual. Quantitative RT-PCR was conducted using Prelude™ PreAmp Master Mix (Takara) and CFX96 Real-Time System (Bio-Rad). The sequences of all the primers were obtained from the National Centre for Biotechnology Information (NCBI) database and listed in Supplementary Material Table 1. The expressions of all genes were normalized to human or mouse glyceraldehyde 3-phosphate dehydrogenase (GAPDH).

Immunoblotting analysis: Tumor cells were collected after various treatments and then lysed by Pierce™ RIPA Buffer (Thermo Scientific) supplemented with Halt™ Phosphatase Inhibitor Cocktail (Thermo Fisher). The concentration of protein was determined by the BCA protein assay kit (Solarbio). 50 μg of total protein was loaded in 10% SDS-PAGE gel and then transferred to a nitrocellulose membrane using Trans-Blot Turbo (BIO-RAD). The membrane was blocked with TBST/5% BSA (Solarbio) and incubated with primary antibodies (GAPDH, Bmi1, CXCR4, PI3K, p-PI3K) (Abcam) overnight in 4°C according to the manufacturer's instructions. Then the membrane was incubated with

secondary antibodies (Goat Anti-Rabbit IgG (H + L)-HRP Conjugate, Goat Anti-Mouse IgG (H + L)-HRP Conjugate) (BIO-RAD) at room temperature for 2 h. Before images were taken using ChemiDoc™ MP Imaging System (BIO-RAD, the membrane was immersed with Clarity Max™ Western ECL Blotting Substrates (BIO-RAD) in the dark.

Immunofluorescence staining: Tumor cells were seeded on coverslips and then fixed with 4 % Paraformaldehyde Solution (PFA) (Thermo Scientific™) for 15 min. To block and permeabilize the tumor cells, 0.1% Triton X-100 (SAFC) in 1% BSA solution was added to the coverslips for 1 h at room temperature. Tumor cells were stained with the primary antibody: CXCR4 (Abcam), PI3K (Abcam), and p-PI3K (Abcam) at 4°c overnight and then stained with the corresponding secondary antibody: Goat Anti-Mouse IgG H&L (Alexa Fluor® 488) (Abcam); Goat Anti-Rabbit IgG H&L (Alexa Fluor® 594) (Abcam) at room temperature for 1 h. Cells were washed with PBS for 3 times between each step and immersed in ProLong Gold Antifade Mountant with DAPI (Thermo Fisher Scientific). At least 50 cells/condition were imaged by the fluorescent microscope (Nikon) using PE, FITC, and DAPI channels, respectively. ImageJ (NIH) was utilized to analyze the fluorescence intensity.

Cell viability measurement: MTS assay was adopted to measure cell viability. 100 µl of well-mixed cell solution was collected and then added to a well of 96-well plate. After incubation for 12 h, 20 µl of 5 mg/ml CellTiter 96 Aqueous One Solution (Promega, USA) was added to each well and the plate was incubated at 37°C for 4 h in dark. The absorbance of the cell solution was detected at 492 nm by Labexim Products LEDETECT 96 microplate reader (Labexim, Austria). To calculate the relative cell viability, the absorbance of tumor cells after various treatments were divided by the absorbance of cell solution without treatment.

Cell transfection: The siRNAs of CXCR4 (human and mouse) were purchased from HANBIO (Shanghai, China). Breast cancer cells were plated in 6 well culture plates until they reached 50%-70% confluency. siRNAs were mixed with Opti-MEM (Gibco, USA) and Lipofectamine 3000 Reagent (Thermo Fisher, Waltham, MA, USA) and incubated at room temperature for 15 min. The mixture was added to cancer cells for transfection for 48 h at 37°C. The transfection efficiency was quantified by RT-PCR.

Pharmacologic treatment: Breast cancer cells circulated with or without 0 and 20 dyne/cm^2 shear stress were treated with CXCR4 inhibitor AMD3100 (Sigma-Aldrich), PI3K inhibitor Ly294002 (Invitrogen) for 48 h, and PI3K activator Insulin receptor substrate (Tyr608) peptide (Enzo Life Sciences) for 24 h.

Preparation of tumor-initiating cells: SKBR3 cells were harvested and resuspended into the 3D Tumorsphere medium XF (PromoCell). 30,000 tumor cells in a 3 ml culture medium were added into each well of the ultra-low attachment plate (Corning). These cells were passaged every 4 days. In brief, the tumor spheres were collected in a 15-ml centrifuge tube and placed at room temperature for sedimentation for 10 min. The supernatant was gently removed, and trypsin was added to the tube to break down the tumor sphere. The single tumor cell solution was collected, and the tumor cells were re-suspended in the 3D Tumorsphere medium and seeded in an ultra-low attachment plate to culture for 12 days.

Mice experiment: All animal experiments were approved by the Animal Subjects Ethics Sub-committee of the Hong Kong Polytechnic University. In the subcutaneous xenograft model, $1*10^6$ of SKBR3 cells, TICs, and 0 or 20 dyne/cm^2 shear stress-treated cells in 100 µl Matrigel solution were subcutaneously injected into 4-8 weeks female nude mice. After 2 weeks of implantation, the tumor volume was measured by caliper every 4 days until Day 34 and calculated as V=1/2*W*W*L. W was the shorter diameter of the tumor cross-section and L was the longer diameter of the tumor cross-section. At day 34, the mice were sacrificed, and tumor tissue was collected to measure the tumor weight.

In the intracardiac xenograft model, female nude mice were anesthetized by intra-peritoneal injection of ketamine/xylazine solution. 100 µl of PBS solution containing $1*10^5$ of luciferase labelled MDA-MB-231 cells and 0 or 20 dyne/cm^2 shear stress selected tumor cells was injected into the left ventricle of the heart. Images were taken by Perkin-Elmer IVIS Lumina Series III Pre-clinical In Vivo Animal Imaging Systems after injection to confirm that the tumor cells were successfully injected and spread throughout the whole body. The metastatic tumors at different organs were imaged by this system every week.

For orthotopic injection, ketamine/xylazine solution was injected into the abdomen to anesthetize the mice. $1*10^6$ of luciferase labelled 4T1 cells and 0 or 20 dyne/cm^2 shear stress selected tumor cells were implanted into the 4th mammary fat pad of female nude mice. The primary tumor volume was monitored by a caliper. Once the tumor size reached 500 mm^3, the mice were anesthetized, and the primary tumor was removed. Four days after primary tumor removal, the metastases at different organs were imaged by Perkin-Elmer IVIS Lumina Series III Pre-clinical In Vivo Animal Imaging Systems, and the metastasis was continuously measured every 4 days.

Metastasis-free survival: The database GSE2034 from the Gene Expression Omnibus (GEO) was adopted to test the clinical association between CXCR4 expression and metastasis risk. The gene expression arrays were conducted using the Affymetrix Human Genome U133A array. The patients were split into three tertile groups according to the CXCR4 expression level. The group with high/low CXCR4 expression (High-CXCR4 and Low-CXCR4) represented cancer patients in the highest/lowest tertile.

Statistical analysis: All data were presented as the mean ± standard error of the mean (SEM) and the statistics were analyzed by GraphPad Prism 7 (San Diego, CA, USA). The statistics between two groups were analyzed by non-paired student t-test and for three groups or more, one-way ANOVA tests were performed. The post hoc Bonferroni test was adopted in the ANOVA analysis. The statistical analysis in the metastasis-free survival curve was conducted using the log–rank (Mantel–Cox) test. $*$, $p < 0.05$, $**$, $p < 0.01$, $***$, $p < 0.001$, $****$, $p < 0.0001$.

Acknowledgements

We thank the University Life Science Facility in the Hong Kong Polytechnic University for providing the confocal laser scanning microscopy, flow cytometry, and central animal facility. We acknowledge the support from National Natural Science Foundation of China (Project no. 11972316), Shenzhen Science and Technology Innovation Commission (Project no. JCYJ20200109142001798,

SGDX2020110309520303, and JCYJ20220531091002006), General Research Fund of Hong Kong Research Grant Council (PolyU 15214320 and 15227523), Health and Medical Research Fund (18191421), and the internal grants from the Hong Kong Polytechnic University (1-ZE2M, 1-CD75, and 1-ZVY1).

CRediT authorship contribution statement

Ying Xin: Methodology, Formal analysis, Data curation, Writing – review & editing. **Bing Hu**: Investigation, Methodology. **Keming Li**: Validation, Data curation. **Guanshuo Hu**: Investigation, Methodology. **Cunyu Zhang**: Investigation. **Xi Chen**: Methodology. **Kai Tang**: Investigation. **Pengyu Du**: Investigation. **Youhua Tan**: Investigation, Methodology, Supervision, Project administration, Conceptualization. Writing – review & editing.

Competing Interests

The authors declare no competing financial interest.

Supplementary Material

The Supplementary material includes 6 supplementary figures and 1 table.

References:

1. Yang, C., et al., *Circulating tumor cells in precision oncology: clinical applications in liquid biopsy and 3D organoid model.* Cancer Cell International, 2019. **19**(1): p. 341.
2. Massagué, J. and K. Ganesh, *Metastasis-Initiating Cells and Ecosystems.* Cancer Discov, 2021. **11**(4): p. 971-994.
3. Li, K., et al., *Desmosomal proteins of DSC2 and PKP1 promote cancer cells survival and metastasis by increasing cluster formation in circulatory system.* Science advances, 2021. **7**(40): p. eabg7265-eabg7265.
4. Massagué, J. and A.C. Obenauf, *Metastatic colonization by circulating tumour cells.* Nature, 2016. **529**(7586): p. 298-306.
5. Chambers, A.F., A.C. Groom, and I.C. MacDonald, *Dissemination and growth of cancer cells in metastatic sites.* Nat Rev Cancer, 2002. **2**(8): p. 563-72.
6. Luzzi, K.J., et al., *Multistep nature of metastatic inefficiency: dormancy of solitary cells after successful extravasation and limited survival of early micrometastases.* Am J Pathol, 1998. **153**(3): p. 865-73.

7. Wang, R., et al., *The Clinicopathological features and survival outcomes of patients with different metastatic sites in stage IV breast cancer.* BMC Cancer, 2019. **19**(1): p. 1091.
8. Valastyan, S. and R.A. Weinberg, *Tumor metastasis: molecular insights and evolving paradigms.* Cell, 2011. **147**(2): p. 275-292.
9. Celià-Terrassa, T. and Y. Kang, *Distinctive properties of metastasis-initiating cells.* Genes & development, 2016. **30**(8): p. 892-908.
10. Pascual, G., et al., *Targeting metastasis-initiating cells through the fatty acid receptor CD36.* Nature, 2017. **541**(7635): p. 41-45.
11. Ganesh, K., et al., *L1CAM defines the regenerative origin of metastasis-initiating cells in colorectal cancer.* Nat Cancer, 2020. **1**(1): p. 28-45.
12. Oskarsson, T., et al., *Breast cancer cells produce tenascin C as a metastatic niche component to colonize the lungs.* Nat Med, 2011. **17**(7): p. 867-74.
13. Wculek, S.K. and I. Malanchi, *Neutrophils support lung colonization of metastasis-initiating breast cancer cells.* Nature, 2015. **528**(7582): p. 413-417.
14. Baccelli, I., et al., *Identification of a population of blood circulating tumor cells from breast cancer patients that initiates metastasis in a xenograft assay.* Nature Biotechnology, 2013. **31**(6): p. 539-544.
15. Yamashita, D., et al., *Identification of ALDH1A3 as a Viable Therapeutic Target in Breast Cancer Metastasis-Initiating Cells.* Mol Cancer Ther, 2020. **19**(5): p. 1134-1147.
16. Pein, M., et al., *Metastasis-initiating cells induce and exploit a fibroblast niche to fuel malignant colonization of the lungs.* Nature Communications, 2020. **11**(1): p. 1494.
17. Castaño, Z., et al., *IL-1β inflammatory response driven by primary breast cancer prevents metastasis-initiating cell colonization.* Nat Cell Biol, 2018. **20**(9): p. 1084-1097.
18. Xin, Y., et al., *Mechanics and Actomyosin-Dependent Survival/Chemoresistance of Suspended Tumor Cells in Shear Flow.* Biophysical Journal, 2019. **116**(10): p. 1803-1814.
19. Choi, H.Y., et al., *Hydrodynamic shear stress promotes epithelial-mesenchymal transition by downregulating ERK and GSK3β activities.* Breast Cancer Research, 2019. **21**(1): p. 6.
20. Regmi, S., A. Fu, and K.Q. Luo, *High Shear Stresses under Exercise Condition Destroy Circulating Tumor Cells in a Microfluidic System.* Scientific Reports, 2017. **7**(1): p. 39975.
21. Yankaskas, C.L., et al., *The fluid shear stress sensor TRPM7 regulates tumor cell intravasation.* Science Advances, 2021. **7**(28): p. eabh3457.
22. Fan, R., et al., *Circulatory shear flow alters the viability and proliferation of circulating colon cancer cells.* Scientific Reports, 2016. **6**(1): p. 27073.
23. Barnes, J.M., J.T. Nauseef, and M.D. Henry, *Resistance to Fluid Shear Stress Is a Conserved Biophysical Property of Malignant Cells.* PLOS ONE, 2012. **7**(12): p. e50973.
24. Hope, J.M., et al., *Circulating prostate cancer cells have differential resistance to fluid shear stress-induced cell death.* Journal of Cell Science, 2021. **134**(4): p. jcs251470.
25. Ma, S., et al., *Hemodynamic shear stress stimulates migration and extravasation of tumor cells by elevating cellular oxidative level.* Cancer Lett, 2017. **388**: p. 239-248.
26. Marrella, A., et al., *High blood flow shear stress values are associated with circulating tumor cells cluster disaggregation in a multi-channel microfluidic device.* PLOS ONE, 2021. **16**(1): p. e0245536.
27. Mitchell, M.J., et al., *Lamin A/C deficiency reduces circulating tumor cell resistance to fluid shear stress.* American journal of physiology. Cell physiology, 2015. **309**(11): p. C736-C746.
28. Moose, D.L., et al., *Cancer Cells Resist Mechanical Destruction in Circulation via RhoA/Actomyosin-Dependent Mechano-Adaptation.* Cell Reports, 2020. **30**(11): p. 3864-3874.e6.
29. Huang, Q., et al., *Shear stress activates ATOH8 via autocrine VEGF promoting glycolysis dependent-survival of colorectal cancer cells in the circulation.* Journal of Experimental & Clinical Cancer Research, 2020. **39**(1): p. 25.
30. Furlow, P.W., et al., *Mechanosensitive pannexin-1 channels mediate microvascular metastatic cell survival.* Nat Cell Biol, 2015. **17**(7): p. 943-52.
31. Huang, Q., et al., *Fluid shear stress and tumor metastasis.* American journal of cancer research, 2018. **8**(5): p. 763-777.

32. Meng, S., et al., *Circulating Tumor Cells in Patients with Breast Cancer Dormancy.* Clinical Cancer Research, 2004. **10**(24): p. 8152.
33. Jin, J., et al., *Hemodynamic shear flow regulates biophysical characteristics and functions of circulating breast tumor cells reminiscent of brain metastasis.* Soft Matter, 2018. **14**(47): p. 9528-9533.
34. Xin, Y., et al., *Fluid Shear Stress Induces EMT of Circulating Tumor Cells via JNK Signaling in Favor of Their Survival during Hematogenous Dissemination.* International Journal of Molecular Sciences, 2020. **21**(21).
35. de Beça, F.F., et al., *Cancer stem cells markers CD44, CD24 and ALDH1 in breast cancer special histological types.* J Clin Pathol, 2013. **66**(3): p. 187-91.
36. Wright, M.H., et al., *Brca1 breast tumors contain distinct CD44+/CD24- and CD133+ cells with cancer stem cell characteristics.* Breast Cancer Res, 2008. **10**(1): p. R10.
37. Xin, Y., et al., *Biophysics in tumor growth and progression: from single mechano-sensitive molecules to mechanomedicine.* Oncogene, 2023.
38. Chen, X., et al., *Biomechanics of cancer stem cells.* Essays in Biochemistry, 2022. **66**(4): p. 359-369.
39. Tan, Y., et al., *The mechanics of tumor cells dictate malignancy via cytoskeleton-mediated APC/Wnt/β-catenin signaling.* Research. **0**(ja).
40. Wang, J., et al., *Cell mechanics regulate the migration and invasion of hepatocellular carcinoma cells via JNK signaling.* Acta Biomaterialia, 2024. **176**: p. 321-333.
41. Buonomo, O.C., et al., *New insights into the metastatic behavior after breast cancer surgery, according to well-established clinicopathological variables and molecular subtypes.* PloS one, 2017. **12**(9): p. e0184680-e0184680.
42. Chen, X., et al., *Mechanical Heterogeneity in the Bone Microenvironment as Characterized by Atomic Force Microscopy.* Biophysical Journal, 2020. **119**(3): p. 502-513.
43. da Silva-Diz, V., et al., *Cancer cell plasticity: Impact on tumor progression and therapy response.* Semin Cancer Biol, 2018. **53**: p. 48-58.
44. Calibasi Kocal, G., et al., *Dynamic Microenvironment Induces Phenotypic Plasticity of Esophageal Cancer Cells Under Flow.* Scientific Reports, 2016. **6**(1): p. 38221.
45. Discher, D.E., P. Janmey, and Y.L. Wang, *Tissue cells feel and respond to the stiffness of their substrate.* Science, 2005. **310**(5751): p. 1139-43.
46. Yang, N., et al., *CXCR4 mediates matrix stiffness-induced downregulation of UBTD1 driving hepatocellular carcinoma progression via YAP signaling pathway.* Theranostics, 2020. **10**(13): p. 5790-5801.
47. Wang, B., P. Guo, and D.T. Auguste, *Mapping the CXCR4 receptor on breast cancer cells.* Biomaterials, 2015. **57**: p. 161-168.
48. Sun, X., et al., *CXCR4/SDF1 mediate hypoxia induced chondrosarcoma cell invasion through ERK signaling and increased MMP1 expression.* Molecular Cancer, 2010. **9**(1): p. 17.
49. Sobolik, T., et al., *CXCR4 drives the metastatic phenotype in breast cancer through induction of CXCR2 and activation of MEK and PI3K pathways.* Molecular Biology of the Cell, 2014. **25**(5): p. 566-582.
50. Munson, J.M., R.V. Bellamkonda, and M.A. Swartz, *Interstitial flow in a 3D microenvironment increases glioma invasion by a CXCR4-dependent mechanism.* Cancer Res, 2013. **73**(5): p. 1536-46.
51. Neves, S.R., P.T. Ram, and R. Iyengar, *G Protein Pathways.* Science, 2002. **296**(5573): p. 1636.
52. Alhadeff, R., et al., *Exploring the free-energy landscape of GPCR activation.* Proceedings of the National Academy of Sciences, 2018. **115**(41): p. 10327.
53. She, Q.-B., et al., *Breast Tumor Cells with PI3K Mutation or HER2 Amplification Are Selectively Addicted to Akt Signaling.* PLOS ONE, 2008. **3**(8): p. e3065.
54. Sun, B., et al., *Oridonin inhibits aberrant AKT activation in breast cancer.* Oncotarget, 2018. **9**(35).
55. Azevedo, A.S., et al., *Metastasis of circulating tumor cells: Favorable soil or suitable biomechanics, or both?* Cell Adhesion & Migration, 2015. **9**(5): p. 345-356.
56. Fares, J., et al., *Molecular principles of metastasis: a hallmark of cancer revisited.* Signal Transduction and Targeted Therapy, 2020. **5**(1): p. 28.

57. Kumar, S. and V.M. Weaver, *Mechanics, malignancy, and metastasis: the force journey of a tumor cell.* Cancer Metastasis Rev, 2009. **28**(1-2): p. 113-27.
58. Follain, G., et al., *Fluids and their mechanics in tumour transit: shaping metastasis.* Nat Rev Cancer, 2020. **20**(2): p. 107-124.
59. Xu, Z., et al., *Fluid shear stress regulates the survival of circulating tumor cells via nuclear expansion.* Journal of Cell Science, 2022. **135**(10): p. jcs259586.
60. Moose, D.L., et al., *Abstract B047: Fluid shear stress enhances the metastatic potential and rapidly alters metabolism of circulating tumor cells.* Cancer Research, 2023. **83**(2_Supplement_2): p. B047-B047.
61. Alvarado-Estrada, K., et al., *Circulatory shear stress induces molecular changes and side population enrichment in primary tumor-derived lung cancer cells with higher metastatic potential.* Scientific Reports, 2021. **11**(1): p. 2800.
62. Lin, C.W., et al., *Immunity against cancer cells may promote their proliferation and metastasis.* Proc Natl Acad Sci U S A, 2020. **117**(1): p. 426-431.
63. Wang, N., J.D. Tytell, and D.E. Ingber, *Mechanotransduction at a distance: mechanically coupling the extracellular matrix with the nucleus.* Nat Rev Mol Cell Biol, 2009. **10**(1): p. 75-82.
64. Kamal, M. and R. Jockers, *Biological Significance of GPCR Heteromerization in the Neuro-Endocrine System.* Frontiers in endocrinology, 2011. **2**: p. 2-2.
65. Pierce, K.L., R.T. Premont, and R.J. Lefkowitz, *Seven-transmembrane receptors.* Nature Reviews Molecular Cell Biology, 2002. **3**(9): p. 639-650.
66. Cahalan, S.M., et al., *Piezo1 links mechanical forces to red blood cell volume.* eLife, 2015. **4**: p. e07370.
67. Xu, J., et al., *GPR68 Senses Flow and Is Essential for Vascular Physiology.* Cell, 2018. **173**(3): p. 762-775.e16.
68. Sangha, G.S., et al., *Mechanical stimuli such as shear stress and piezo1 stimulation generate red blood cell extracellular vesicles.* Frontiers in Physiology, 2023. **14**.
69. Shah, A.D., M.J. Bouchard, and A.C. Shieh, *Interstitial Fluid Flow Increases Hepatocellular Carcinoma Cell Invasion through CXCR4/CXCL12 and MEK/ERK Signaling.* PLoS One, 2015. **10**(11): p. e0142337.
70. Xiang, Z.-l., et al., *Chemokine receptor CXCR4 expression in hepatocellular carcinoma patients increases the risk of bone metastases and poor survival.* BMC Cancer, 2009. **9**(1): p. 176.
71. Maréchal, R., et al., *High expression of CXCR4 may predict poor survival in resected pancreatic adenocarcinoma.* British Journal of Cancer, 2009. **100**(9): p. 1444-1451.
72. Bert, M., et al. *High-resolution tomographic imaging of microvessels*. in *Proc.SPIE*. 2008.
73. Pereira-Veiga, T., et al., *Circulating tumor cell-blood cell crosstalk: Biology and clinical relevance.* Cell Rep, 2022. **40**(9): p. 111298.
74. Dianat-Moghadam, H., et al., *NK cells-directed therapies target circulating tumor cells and metastasis.* Cancer Lett, 2021. **497**: p. 41-53.
75. von Tempelhoff, G.F., et al., *Association between blood rheology, thrombosis and cancer survival in patients with gynecologic malignancy.* Clin Hemorheol Microcirc, 2000. **22**(2): p. 107-30.
76. Alix-Panabières, C. and K. Pantel, *Challenges in circulating tumour cell research.* Nat Rev Cancer, 2014. **14**(9): p. 623-31.
77. Khoo, B.L., et al., *Liquid biopsy and therapeutic response: Circulating tumor cell cultures for evaluation of anticancer treatment.* Sci Adv, 2016. **2**(7): p. e1600274.
78. Borowicz, S., et al., *The soft agar colony formation assay.* Journal of visualized experiments : JoVE, 2014(92): p. e51998.
79. Liu, J., et al., *Soft fibrin gels promote selection and growth of tumorigenic cells.* Nat Mater, 2012. **11**(8): p. 734-41.

Figure Legends

Fig. 1 FSS enriches a subpopulation of CTCs with enhanced stemness, migration, and invasion ability. (a) A schematic diagram showing the rate-limiting role of FSS in hematogenous dissemination of CTCs from a primary lesion to distal organs. (b) The adhesion of shear-selected tumor cells or ssMICs to the endothelial monolayer. ssMICs, suspension control, and control cells were labelled with fluorescent dye and attached to the HUVEC monolayer for 1, 2, 4, and 8 h, respectively. The number of adhered cells was counted. n=3 independent experiments. Scale bar: 50 μm. (c) Transendothelial migration of ssMICs. HUVEC were seeded on a Transwell insert membrane to form an intact monolayer. Fluorescent-labeled ssMICs, suspension control, and control tumor cells were added to the top chamber of the Transwell. After 48 h, those tumor cells which migrated through the endothelium were imaged and counted. n=3 independent experiments. Scale bar: 50 μm. (d) The migration ability of ssMICs. The migration ability of tumor cells was measured by Transwell migration assay. n=3 independent experiments. Scale bar: 50 μm. (e) The invasion of ssMICs in 3D collagen. The indicated cells were utilized to generate tumor spheroids in suspension culture, the invasion of which was then examined in 3D collagen gels at 12 and 24 h, respectively. The invasion index was calculated as the invasion area divided by the initial spheroid area. n=3 independent experiments. Scale bar: 500 μm. (f) The anchorage-independent growth of ssMICs. The indicated cells were cultured in soft agar and the number of the generated colonies was counted at day 14. n=3 independent experiments. (g-j) The expressions of the markers related to stemness and metastasis in ssMICs. The expressions of the corresponding markers were analyzed by flow cytometry (g and h), qPCR (i), and immunoblotting (j), respectively. n=3 independent experiments in (i); (g, h, j): representative of two independent experiments. The ANOVA analysis was utilized for the statistics in (b-f) and (i) and Bonferroni test was adopted for post hoc analysis. *, $p<0.05$; **, $p<0.01$; ***, $p<0.001$; ****, $p<0.0001$.

Fig. 2 Shear-selected tumor cells exhibit metastasis-initiating ability *in vivo*. (a) Tumor growth curves of ssMICs in a subcutaneous model. TICs were obtained from the mammosphere growth of

SKBR3 cells in low-attachment plates. ssMICs, suspension control, control cells, and TICs were then injected subcutaneously into female nude mice (n=6 per condition). The tumor volume was measured at the indicated time points. (b) The weight of the generated tumors. The xenografts in (a) were retrieved and weighed at day 34. Scale bar: 1 cm. (c) Tumor growth in an orthotopic model. ssMICs, suspension control, and control 4T1 cells were injected into the mammary fat pad of female nude mice. The tumor volume was measured at day 14. (d) Representative images of the resected tumor tissues. Scale bar: 1 cm. (e-h) The incidence of metastases in various organs after the resection of primary tumors. In (c), once the tumor size reached 500 mm^3, the generated xenografts were surgically removed and the generation of tumor metastases was monitored starting from day 4 after the tumor removal by bioluminescence imaging (e, f). The bioluminescence intensity at day 20 was compared among ssMIC, suspension control, and control cells (g). The incidence of metastases was analysed at different organs (h). n=4 for each condition. The ANOVA analysis was utilized for the statistics in (a-c, f, and g) and Bonferroni test was adopted for post hoc analysis. *, $p<0.05$; **, $p<0.01$; ***, $p<0.001$. In (a), blue or red stars represent the comparison between "Control" and "ssMIC" or "TIC".

Fig. 3 ssMICs display characteristic biophysical properties and cellular plasticity. (a) The proliferation of ssMICs on the substrates mimicking the mechanics of bone, liver, and lung tissue. ssMIC, suspension control, and control cells were cultured on 5 and 35 kPa PA hydrogels for 48 h. Cell proliferation was analyzed by EdU assay and flow cytometry. n=2 independent experiments. (b) The contractility of ssMICs. The indicated cells were placed on 35 kPa hydrogels for 12 h. The contractility was measuredy by traction force microscopy. n>15 cells per condition. (c-e) The cytoskeleton and stiffness of ssMICs. The indicated cells were cultured on glass for 12 h, when F-actin was measured by immunofluorescence staining (c, d) and cellular stiffness (e) was measured by atomic force microscopy. n>40 and 67 cells in (d) and (e). Scale bar: 50 μm in (c). (f) The percentage of CD133+ subpopulation after the culture of ssMICs on glass for 7 days. ssMIC, suspension control, and control cells were cultured on glass for 0 and 7 days, when the percentage of CD133+ cells was measured by flow

cytometry. n=2 independent experiments. (g) The plasticity of ssMICs in gene expression. The indicated SKBR3 cells were cultured on glass for 0 and 7 days, respectively. The expressions of stemness and metastatic markers were measured by qPCR. n=3 independent experiments. (h-j) The plasticity of ssMICs in cytoskeleton and cellular stiffness. ssMIC, suspension control, and control SKBR3 cells were cultured on glass for 0, 3, and 6 days, respectively. Cell stiffness, F-actin, and p-MLC were measured by atomic force microscopy and immunofluorescence. At least 50 cells were measured for each condition. The ANOVA analysis was utilized for the statistics in (b, d, e, g, and h-j) and Bonferroni test was adopted for post hoc analysis. *, $p<0.05$; **, $p<0.01$; ***, $p<0.001$; ****, $p<0.0001$.

Fig. 4 FSS enriches ssMICs through the mechanosensitive protein CXCR4. (a-c) The level of CXCR4 in ssMICs. The expression of CXCR4 in ssMIC, suspension control, and control SKBR3 cells was examined by immunofluorescence (a), immunoblotting (b), and flow cytometry (c). n>34 per condition in (a); n=2 independent experiments in (b) and (c). Scale bar: 50 μm in (a). (d-f) The migration and colony formation of tumor cells after knockdown of CXCR4. SKBR3 cells were transfected with CXCR4 siRNA and then treated under 0 and 20 dyne/cm^2 FSS for 12 h. The migration and colony formation of these cells were analyzed in Transwell migration assay (d, e) and soft agar assay (d, f). n=3 independent experiments. Scale bar: 50 μm in (d). (g-i) Cell migration and self-renewal after pharmacologic inhibition of CXCR4. SKBR3 and 4T1 cells were treated with CXCR4 antagonist AMD3100 (10 μM) and then circulated under 0 and 20 dyne/cm^2 FSS for 12 h. The migration and colony formation of these cells were analyzed. n=3 independent experiments. Scale bar: 50 μm in (g). (j-l) The migration and colony formation of ssMICs when CXCR4 is silenced. ssMICs were transfected with CXCR4 siRNA. Cell migration (j, k) and colony formation (j, l) of these cells were then analyzed. n=3 independent experiments. Scale bar: 50 μm in (j). (m) The invasion of ssMICs after CXCR4 inhibition. ssMICs were treated with CXCR4 antagonist AMD3100 (10 μM) and their invasion ability was measured in 3D collagen at 12 and 24 h. Scale bar: 200 μm. The ANOVA analysis was utilized for

the statistics in (a, e, f, h, i, m) and Bonferroni test was adopted for post hoc analysis. Student t-test was used for the statistics in (k and l). *, $p<0.05$; **, $p<0.01$; ***, $p<0.001$; ****, $p<0.0001$.

Fig. 5 FSS selects ssMICs through CXCR4-PI3K-AKT signaling. (a) The percentage of CXCR4+ subpopulation after shear treatment. SKBR3 were sorted into CXCR4+ and CXCR4- cells via FACS, which were then treated under 0 and 20 dyne/cm^2 FSS for 12 h. The percentage of CXCR4+ subpopulation was measured by flow cytometry. n=2 independent experiments. (b) The viability of CXCR4+/- cells under FSS. CXCR4+/- cells were treated under 0 and 20 dyne/cm^2 FSS for 12 h. Cell viability was measured by MTS assay. n=3 independent experiments. (c, d) The migration and colony formation ability of CXCR4- and CXCR4+ cells after shear treatment. CXCR4+/- cells were treated under 0 and 20 dyne/cm^2 FSS for 12 h and their migration (c) and colony formation (d) were then analyzed. n=3 independent experiments. Scale bar: 50 μm in (c). (e) The activity of PI3K signaling in ssMICs. The expressions of PI3K and p-PI3K were analyzed by immunoblotting. n=2 independent experiments. (f-h) The migration and colony formation of tumor cells after the inhibition of PI3K signaling. 4T1 cells were treated with 1 μM LY294002 (PI3K inhibitor) and then treated under 0 and 20 dyne/cm^2 FSS for 12 h. Cell migration and colony formation ability were measured. n=3 independent experiments. Scale bar: 50 μm in (f). (i-k) The effect of PI3K activation on the migration and colony formation of tumor cells with CXCR4 inhibition. 4T1 cells were transfected with CXCR4 siRNA and treated with PI3K activator IRS-1 (Tyr608) peptide. These cells were then treated under 0 and 20 dyne/cm^2 FSS for 12 h. Cell migration (i, j) and colony formation ability (i, k) were measured. n=3 independent experiments. Scale bar: 50 μm in (i). The ANOVA analysis was utilized for the statistics in (b-d, g, h, j, and k) and Bonferroni test was adopted for post hoc analysis. *, $p<0.05$; **, $p<0.01$; ***, $p<0.001$; ****, $p<0.0001$.

853 **Fig. 1**

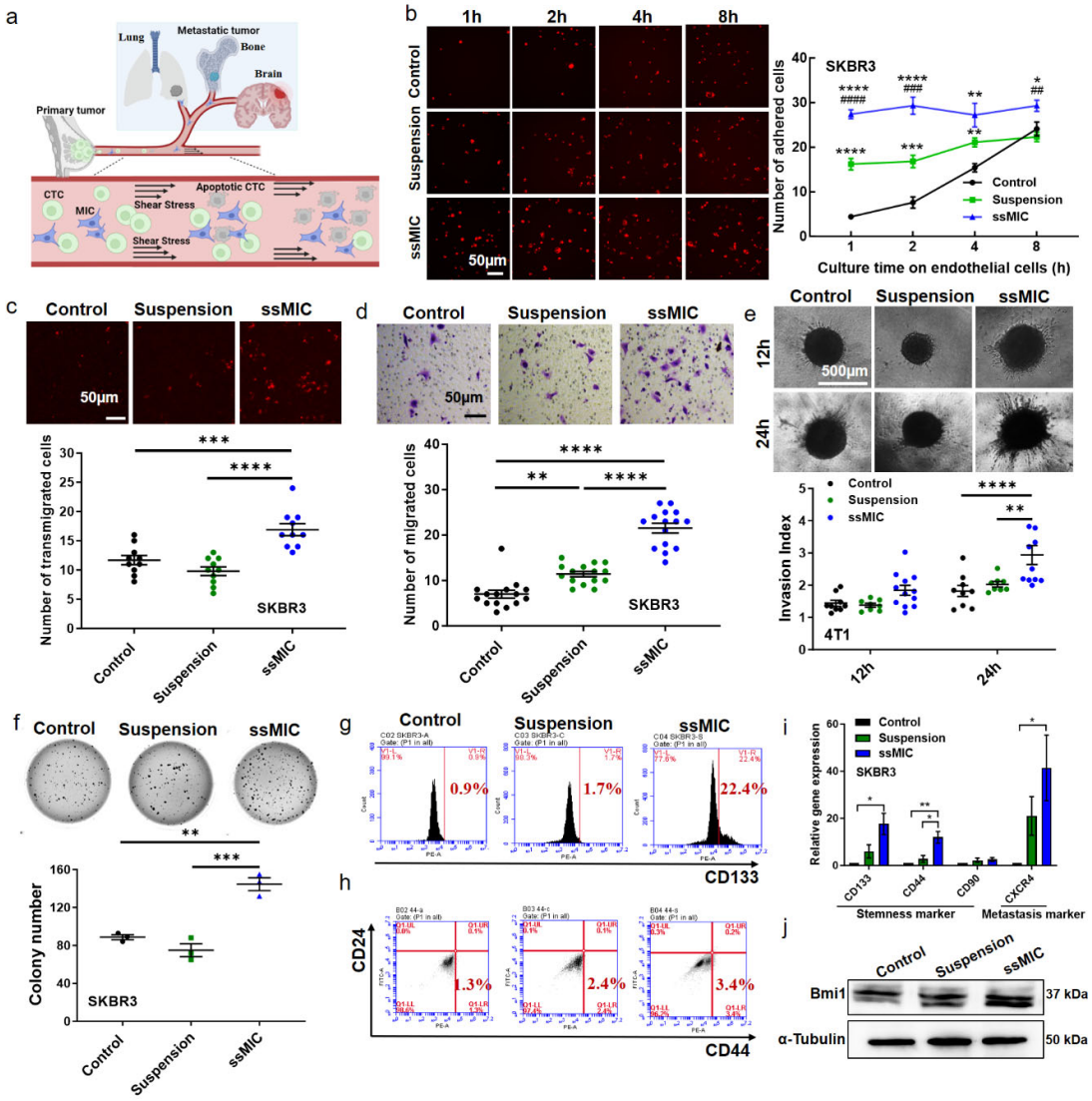

854

855

856

Fig. 2

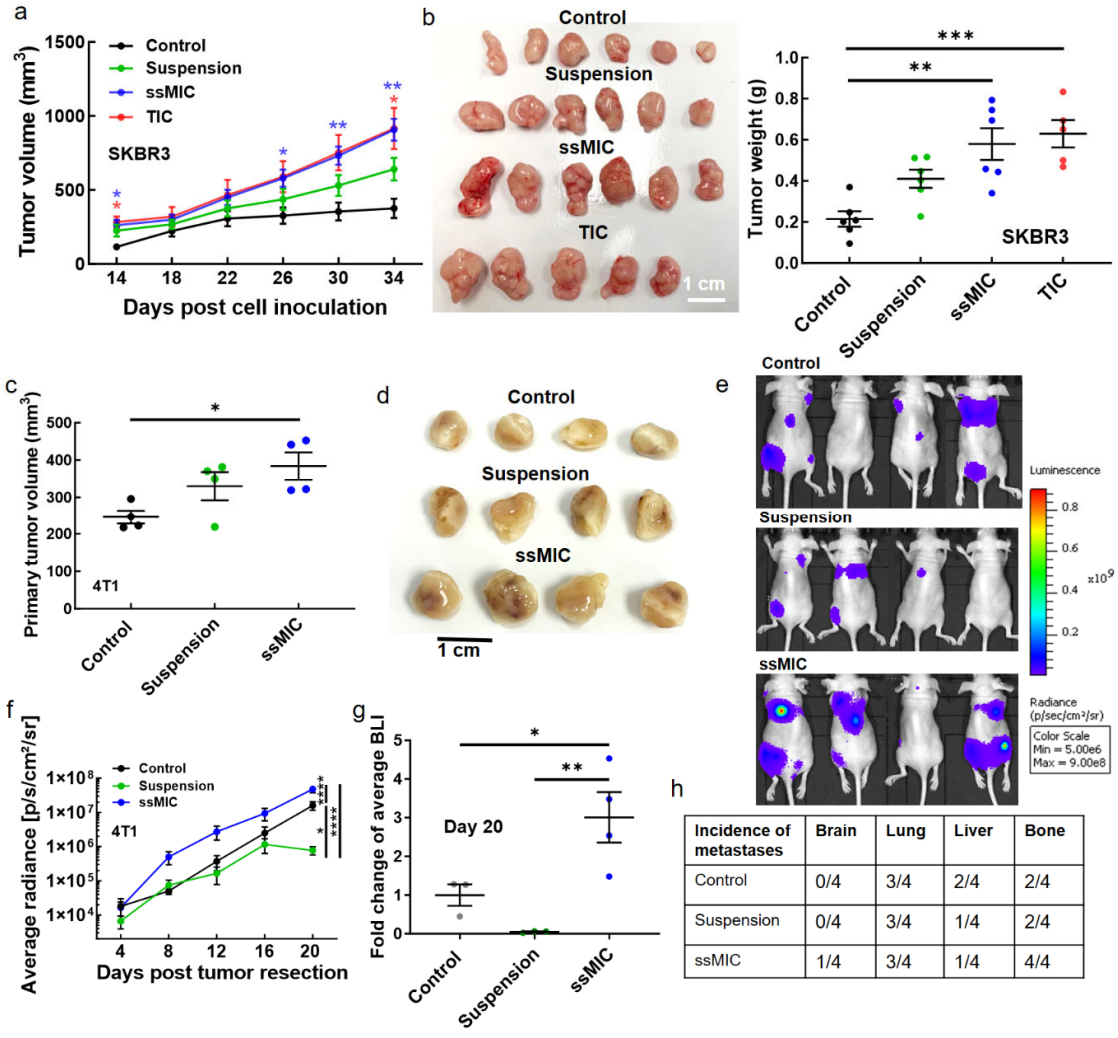

h

Incidence of metastases	Brain	Lung	Liver	Bone
Control	0/4	3/4	2/4	2/4
Suspension	0/4	3/4	1/4	2/4
ssMIC	1/4	3/4	1/4	4/4

Fig. 3

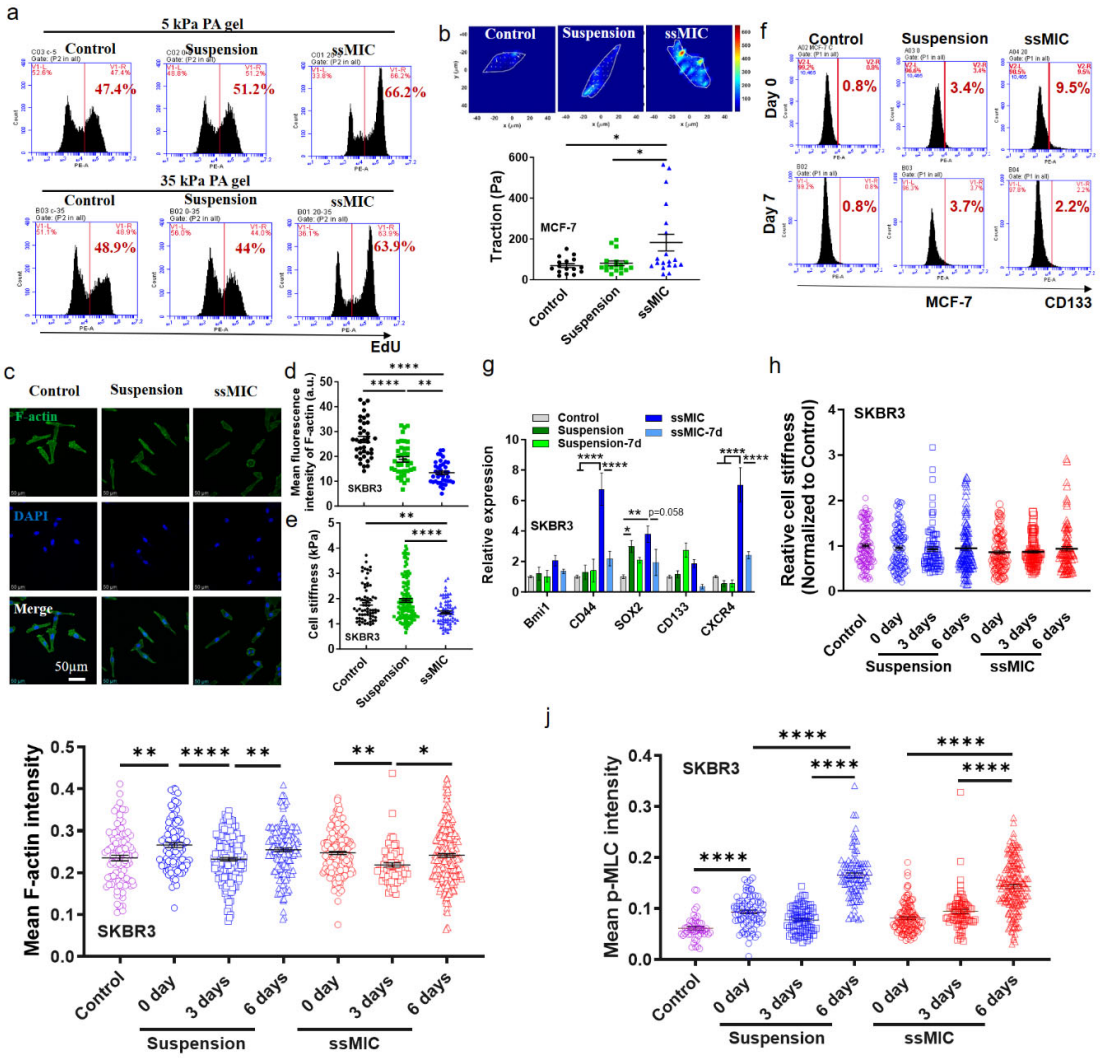
a
5 kPa PA gel
Control
Suspension
ssMIC
47.4%
51.2%
66.2%
35 kPa PA gel
48.9%
44%
63.9%
EdU
b
Control
Suspension
ssMIC
Traction (Pa)
MCF-7
c
F-actin
DAPI
Merge
50μm
d
Mean fluorescence intensity of F-actin (a.u.)
SKBR3
e
Cell stiffness (kPa)
f
Day 0
Day 7
0.8%
3.4%
9.5%
0.8%
3.7%
2.2%
MCF-7
CD133
g
Control
Suspension
Suspension-7d
ssMIC
ssMIC-7d
Relative expression
Bmi1
CD44
SOX2
CD133
CXCR4
p=0.058
h
Reative cell stiffness (Normalized to Control)
0 day
3 days
6 days
Suspension
ssMIC
i
Mean F-actin intensity
j
Mean p-MLC intensity

865 **Fig. 4**

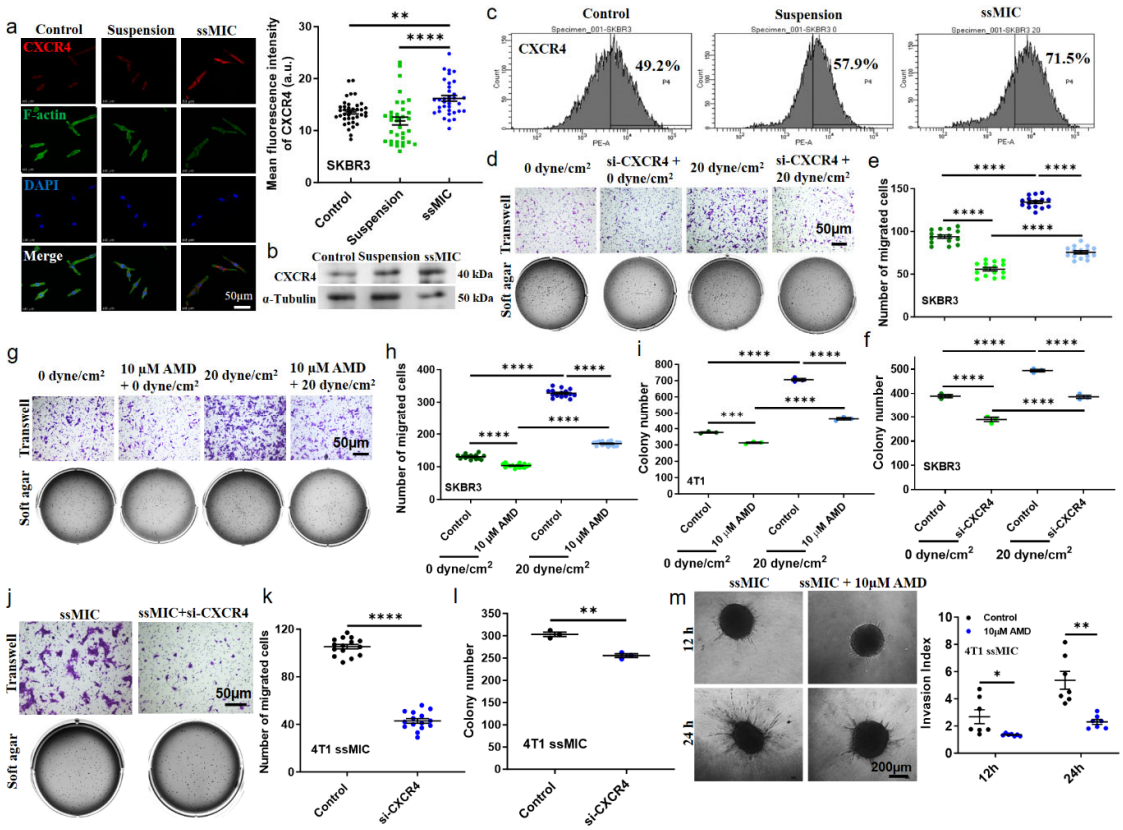

866

867

Fig. 5

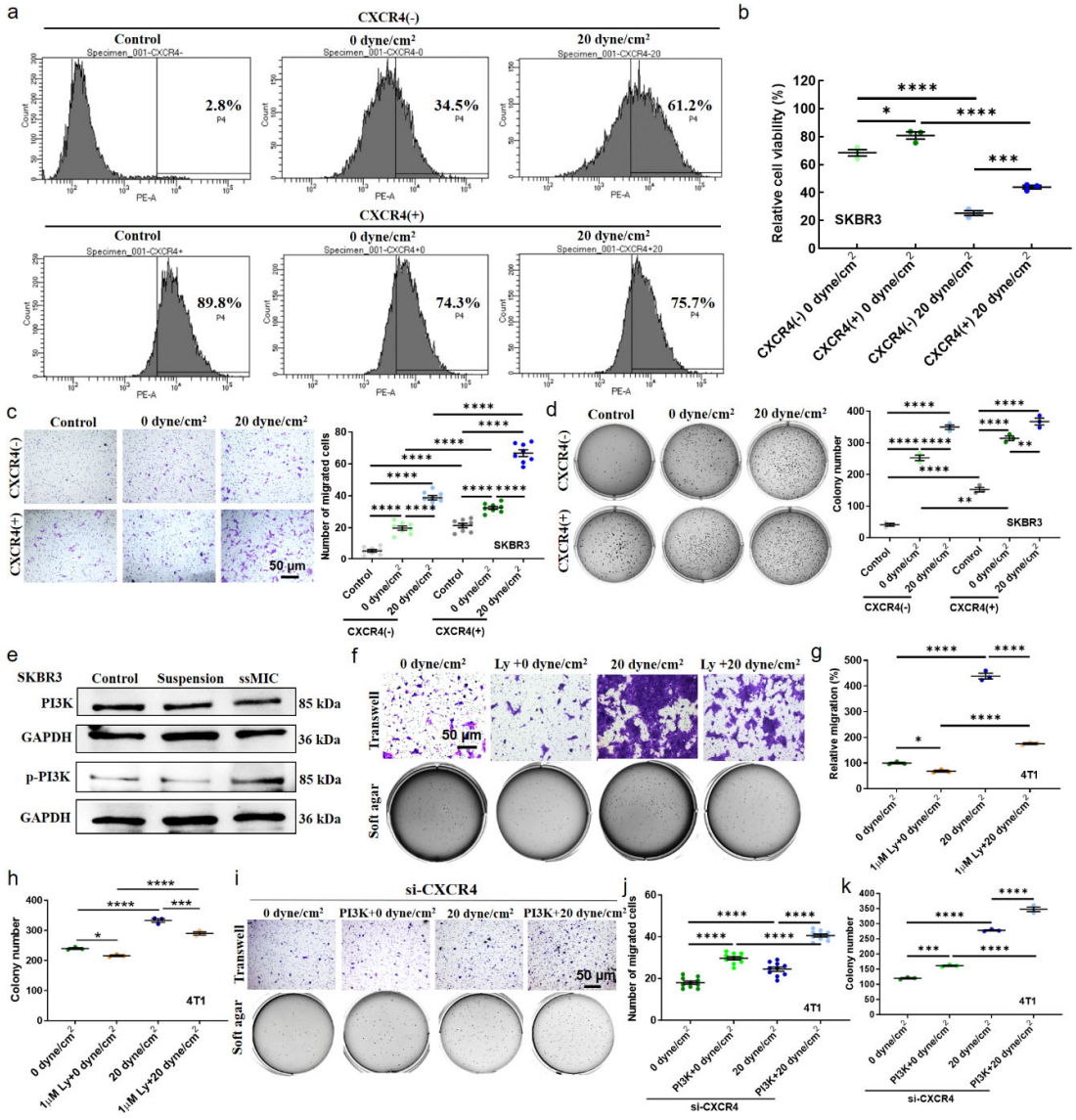
a
CXCR4(-)
Control
0 dyne/cm²
20 dyne/cm²
2.8%
34.5%
61.2%
CXCR4(+)
89.8%
74.3%
75.7%
b
Relative cell viability (%)
SKBR3
CXCR4(-) 0 dyne/cm²
CXCR4(+) 0 dyne/cm²
CXCR4(-) 20 dyne/cm²
CXCR4(+) 20 dyne/cm²
c
50 μm
Number of migrated cells
d
Colony number
e
SKBR3
Control
Suspension
ssMIC
PI3K
GAPDH
p-PI3K
85 kDa
36 kDa
f
Ly +0 dyne/cm²
Ly +20 dyne/cm²
Transwell
Soft agar
g
Relative migration (%)
4T1
1μM Ly+0 dyne/cm²
1μM Ly+20 dyne/cm²
h
i
si-CXCR4
PI3K+0 dyne/cm²
PI3K+20 dyne/cm²
j
k